High-spin structure in ^{157}Er up to and above band termination

A. O. Evans,[1] E. S. Paul,[1] J. Simpson,[2] M. A. Riley,[3] D. E. Appelbe,[2] D. B. Campbell,[3] P. T. W. Choy,[1] R. M. Clark,[4] M. Cromaz,[4] P. Fallon,[4] A. Görgen,[4,*] D. T. Joss,[2,†] I. Y. Lee,[4] A. O. Macchiavelli,[4] P. J. Nolan,[1] A. Pipidis,[3] D. Ward,[4] and I. Ragnarsson[5]

[1]*Oliver Lodge Laboratory, University of Liverpool, Liverpool L69 7ZE, United Kingdom*
[2]*CCLRC Daresbury Laboratory, Daresbury, Warrington WA4 4AD, United Kingdom*
[3]*Department of Physics, Florida State University, Tallahassee, Florida 32306, USA*
[4]*Nuclear Science Division, Lawrence Berkeley National Laboratory, Berkeley, California 94720, USA*
[5]*Department of Mathematical Physics, Lund Institute of Technology, P.O. Box 118, S-22100 Lund, Sweden*

(Received 8 February 2006; published 15 June 2006)

The high-spin structure of ^{157}Er has been greatly expanded using the Gammasphere spectrometer to investigate the ^{114}Cd(^{48}Ca,5n) reaction at 215 MeV. Many new transitions have been placed in a greatly augmented level scheme up to spin 40$\hbar$ with many collective rotational sequences established. With increasing angular momentum, this nucleus undergoes a Coriolis-induced shape transition from a deformed state of collective rotation to a noncollective configuration. This transition manifests itself as favored band termination near $I = 45\hbar$ in three rotational structures. Many weakly populated states lying at high excitation energy that decay into the terminating states have been discovered. Cranked-Nilsson-Strutinsky calculations suggest that the levels that feed the terminating states arise from weakly collective configurations that break the $Z = 64$ semimagic core.

DOI: 10.1103/PhysRevC.73.064303 PACS number(s): 27.70.+q, 21.10.Re, 23.20.Lv, 23.20.En

I. INTRODUCTION

The generation of angular momentum (spin) in the atomic nucleus has long been a topical question in nuclear physics [1], especially at the extreme values now routinely accessible with large highly efficient multidetector γ-ray spectrometers. Heavy rare-earth nuclei with neutron number $N \sim 90$ are amongst the best candidates for the study of normally deformed ($\beta_2 \lesssim 0.2$) level-stucture to high spin above 40$\hbar$. A deformed prolate nucleus can increase its spin by collective rotation about an axis perpendicular to its symmetry axis leading to $I(I+1)$ quantum-rotor behavior and the observation of regular rotational bands. As the angular momentum is increased in this mass region, the prolate nuclei exhibit dramatic Coriolis-induced alignments of both neutron and proton pairs along their yrast lines. As more and more valence nucleons align with the axis of rotation, a larger fraction of the nuclear spin is generated by single-particle *noncollective* contributions. Eventually, the angular momentum is wholly generated by the single-particle contributions of a finite number of valence nucleons outside a closed spherical (doubly magic) core. This spectacular demise of collectivity at high spin reveals the mesoscopic aspects of the atomic nucleus, a finite fermionic system, and is manifest as *band termination* in γ-ray emission spectra when a regular rotational sequences suddenly ends.

High-spin terminating bands in heavy nuclei were first identified in nuclei around $^{158}_{68}$Er$_{90}$ [2–7] at an angular momentum of $\sim 45\hbar$; a recent summary of the field is given in Ref. [8]. While clear examples of the special terminating states have been identified in a number of erbium isotopes, almost nothing is known about the higher-spin states lying above band termination in isotopes close to the textbook example of ^{158}Er [9,10]. Higher spin can only be generated by energetically expensive particle-hole excitations of the spherical nuclear core. The present experiment was undertaken in order to identify and delineate the nuclear excitation spectrum of these core-breaking states and allow comparisons to theoretical predictions.

In this regard, the present paper documents results for ^{157}Er, the odd-A neighbor of ^{158}Er. Previous high-spin work on this nucleus had established two negative-parity band structures up to termination [7]. The present work has extended the positive-parity yrast band up to a third terminating state. Moreover, a large number of weak high-energy transitions has been established feeding into these three terminating states. Cranked Nilsson-Strutinsky calculations have been performed in order to identify the nature of the levels above the terminating states; these results have been recently presented in Ref. [11] and some additional states are added in this work.

II. EXPERIMENTAL DETAILS AND RESULTS

The high-spin structure of ^{157}Er has been studied at the 88 Inch Cyclotron at the Lawrence Berkeley National Laboratory, using the Gammasphere γ-ray spectrometer [12] containing 102 HPGe detectors. A ^{48}Ca beam of energy 215 MeV was used to bombard two stacked thin self-supporting foils of ^{114}Cd, of total thickness 1.1 mg/cm^2. A total of 1.2×10^9 events were recorded to tape when at least seven Compton-suppressed HPGe detectors fired in prompt time coincidence.

*Present address: DAPNIA/SPhN CEA-Saclay, Bat 703 l'Orme des Merisiers, F-91191 Gif-sur-Yvette, France.
†Present address: Oliver Lodge Laboratory, University of Liverpool, Liverpool L69 7ZE, United Kingdom.

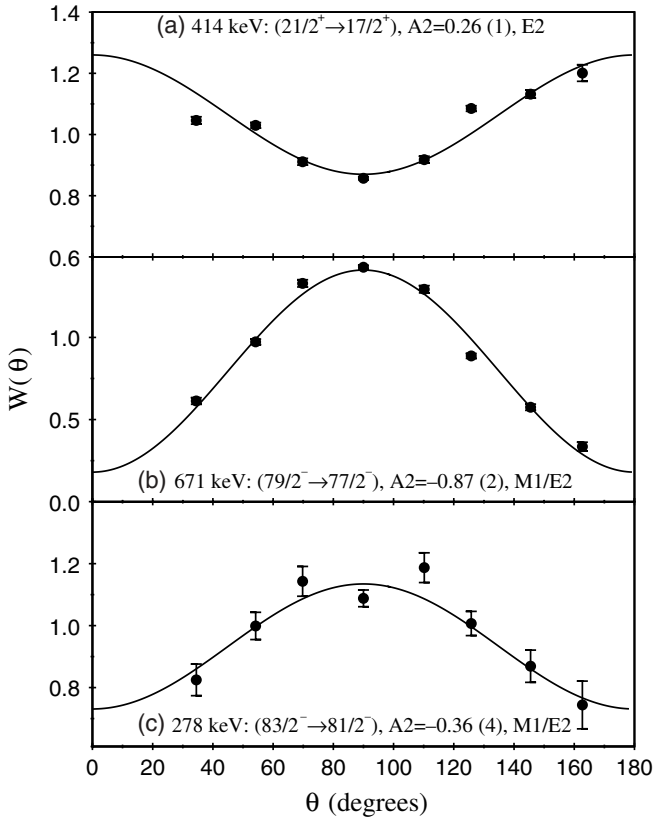

FIG. 1. Typical $\gamma - \gamma$ gated fits of $W(\theta)$ for a stretched $E2$ transition (a) and mixed ($M1/E2$) dipole transitions (b), (c).

In the off-line analysis, approximately 6.5×10^{10} quadruple (γ^4) coincident events were unfolded from the data and replayed into a RADWARE-format four-dimensional hypercube [13,14] for subsequent analysis. In addition, one-dimensional spectra, multiply gated by transitions in ^{157}Er, were unfolded directly from the data [15]. These spectra were also split into the rings of Gammasphere at a fixed angle θ to the beam direction. The intensities of γ-ray transitions measured at a specific angle θ were fitted to the function

$$W(\theta) = 1 + A_2 P_2(\cos\theta) \tag{1}$$

in order to extract A_2 coefficients; stretched quadrupole transitions are characterized by positive A_2 values and pure stretched dipole transitions by negative A_2 values. Figure 1 shows examples of such gated fits for transitions in ^{157}Er. For weak transitions only an angular-intensity ratio

$$R = \frac{I_\gamma, 35^\circ(145^\circ)}{I_\gamma, 90^\circ} \tag{2}$$

could be reliably obtained. Typical angular-intensity ratios extracted from this analysis were $\sim$0.77 for a pure stretched dipole ($\Delta I = 1$) transition, and $\sim$1.33 for a stretched quadrupole ($\Delta I = 2$) transition.

The level scheme deduced for ^{157}Er has been divided into two parts, namely below spin 67/2 and above 65/2, as displayed in Figs. 2 and 3, respectively. The band structures have been labeled Bands 1–10 in order to facilitate the discussion. The measured γ-ray transition energies and relative intensities corresponding to Fig. 2 are listed in Table I, while those corresponding to Fig. 3 are listed in Table II.

A. Low-spin results

1. Bands 1 and 2

Bands 1 and 2 were previously established up to terminating states at $I^\pi = 89/2^-$ and $87/2^-$, respectively [7]. Several newly identified γ rays of energy 328, 327, 322, and 323 keV have been observed decaying from Band 1 into Band 2. Band 2 has been extended down to $I^\pi = 27/2^-$ from the previously observed $I^\pi = 31/2^-$ band head [16] with the addition of a 454 keV quadrupole transition. This new $27/2^-$ state decays to the $25/2^+$ state of Band 3 via a dipole transition of energy 999 keV. A further three new γ rays of energy 429, 451, and 468 keV were observed decaying to the $45/2^+$, $49/2^+$, and $53/2^+$ states of Band 3, respectively, as shown in the spectrum of Fig. 4.

In addition to the 474 keV ($47/2^- \rightarrow 45/2^-$) transition previously identified linking Band 2 to Band 1 [7], seven further transitions with energy 284, 338, 403, 501, 482, 469, and 515 keV have been observed decaying, respectively, from Band 2 into the $I^\pi = 33/2^-, 37/2^-, 41/2^-, 49/2^-, 53/2^-, 57/2^-$, and $61/2^-$ states of Band 1. The establishment of linking transitions between Bands 1 and 2, and the additional links to Band 3, have resulted in a reordering of the transitions in Band 2 between spins $51/2^-$ and $63/2^-$ from the previous work [7].

2. Bands 3 and 4

Bands 3 and 4 where previously established to $I^\pi = 85/2^+$ and (59/2), respectively [7]. The tentative ordering [7,16] of the transitions in Band 3 between $I^\pi = 37/2^+$ and $57/2^+$, due to their similar intensities, has now been confirmed; three γ rays have been observed decaying from Band 2 into this band at spins 45/2, 49/2, and $53/2\hbar$. In addition, transitions feed from Band 4 into Band 3 at spins 45/2, and $49/2\,\hbar$.

Angular-distribution results for transitions linking Bands 4 and 3 suggest positive-parity for Band 4, since $M2$ decay would not be seen in prompt coincidence. This band has been extended to lower spin with the addition of a 345 keV transition and the band head assigned to be $I^\pi = 17/2^+$. This assignment is corroborated by angular-intensity ratios of several of the high energy transitions (>1 MeV) decaying from Band 4 into Band 3; these values are consistent with $\Delta I = 2$ ($E2$) character. The $17/2^+$ state of Band 4 decays to the $13/2^+$ state of Band 3 via a 962 keV transition. A further three ($I \rightarrow I$) transitions of energy 696, 627 and 521 keV, have been observed decaying from the $17/2^+$, $21/2^+$ and $25/2^+$ states of Band 4, respectively, into the $17/2^+$, $21/2^+$ and $25/2^+$ states of Band 3. At higher spin a further two transitions of energy 883 and 933 keV were observed decaying from the $49/2^+$, and $53/2^+$ states of Band 4 into the $45/2^+$ and $49/2^+$ states of Band 3. The multipolarity of the 883 keV $49/2 \rightarrow 45/2^-\gamma$-ray is consistent with stretched $E2$ character.

TABLE I. Energies, intensities and angular-distribution data for the transitions assigned to ^{157}Er which are shown in Fig. 2.

E_γ (keV)[a]	I_γ[b]	A_2[c]	R[d]	Mult.	Assignment	Band
105.3					$25/2^{(-)} \rightarrow 23/2^{(-)}$	$10 \rightarrow 9$
149.6		−0.30(2)	0.81(19)	$M1/E2$	$27/2^{(-)} \rightarrow 25/2^{(-)}$	$9 \rightarrow 10$
157.1	1.7		0.71(11)	$M1/E2$	$9/2^- \rightarrow 7/2^-$	$6 \rightarrow$
181.9					$9/2^- \rightarrow 5/2^-$	6
193.3		−0.18(2)	0.95(2)	$M1/E2$	$29/2^{(-)} \rightarrow 27/2^{(-)}$	$10 \rightarrow 9$
193.3		−0.25(2)	0.95(9)	$M1/E2$	$29/2^- \rightarrow 27/2^-$	$1 \rightarrow 2$
225.2		−0.18(5)	0.84(9)	$M1/E2$	$31/2^{(-)} \rightarrow 29/2^{(-)}$	$9 \rightarrow 10$
231.4	2.3	−0.30(2)	0.71(1)	$M1/E2$	$29/2^- \rightarrow 27/2^{(-)}$	$1 \rightarrow 7$
233.2					$33/2^{(-)} \rightarrow (31/2^-)$	$10 \rightarrow$
252.4	2.3	−0.16(2)	0.79(2)	$M1/E2$	$33/2^- \rightarrow 31/2^-$	$1 \rightarrow 2$
255.0					$27/2^{(-)} \rightarrow 23/2^{(-)}$	9
260					$31/2^- \rightarrow 29/2^-$	$2 \rightarrow 1$
261.0		−0.04(4)	0.89(5)	$M1/E2$	$33/2^{(-)} \rightarrow 31/2^{(-)}$	$10 \rightarrow 9$
265.7	≡100	0.18(1)	1.20(1)	$E2$	$17/2^+ \rightarrow 13/2^+$	3
281.4			0.69(14)	$E1$	$43/2^- \rightarrow 41/2^+$	$2 \rightarrow 4$
283.5			0.88(21)	$M1/E2$	$35/2^- \rightarrow 33/2^-$	$2 \rightarrow 1$
284.8		−0.01(4)	0.92(4)	$M1/E2$	$35/2^{(-)} \rightarrow 33/2^{(-)}$	$9 \rightarrow 10$
290.0	1.5	−0.08(3)	0.89(3)	$M1/E2$	$37/2^- \rightarrow 35/2^-$	$1 \rightarrow 2$
303.2					$39/2^- \rightarrow 37/2^+$	$2 \rightarrow 4$
307.5		−0.04(4)	0.88(4)	$M1/E2$	$37/2^{(-)} \rightarrow 35/2^{(-)}$	$10 \rightarrow 9$
312.6	1.4	−0.12(5)	0.89(5)	$M1/E2$	$41/2^- \rightarrow 39/2^-$	$1 \rightarrow 2$
321.8					$57/2^- \rightarrow 55/2^-$	$1 \rightarrow 2$
323.1					$61/2^- \rightarrow 59/2^-$	$1 \rightarrow 2$
325.2					$45/2^- \rightarrow 43/2^-$	$1 \rightarrow 2$
327.2					$53/2^- \rightarrow 51/2^-$	$1 \rightarrow 2$
327.7					$49/2^- \rightarrow 47/2^-$	$1 \rightarrow 2$
331.6		−0.13(4)	0.94(4)	$M1/E2$	$39/2^{(-)} \rightarrow 37/2^{(-)}$	$9 \rightarrow 10$
338.4		−0.19(1)	0.92(9)	$M1/E2$	$39/2^- \rightarrow 37/2^-$	$2 \rightarrow 1$
343.2					$29/2^{(-)} \rightarrow 25/2^{(-)}$	9
344.8					$21/2^+ \rightarrow 17/2^+$	4
347.5		−0.05(5)	0.90(5)	$M1/E2$	$41/2^{(-)} \rightarrow 39/2^{(-)}$	$10 \rightarrow 9$
352.8		−0.03(6)	0.76(4)	$E1$	$35/2^- \rightarrow 33/2^+$	$2 \rightarrow 4$
362.2	5.1	−0.31(2)	0.73(1)	$M1/E2$	$25/2^- \rightarrow 23/2^{(-)}$	$1 \rightarrow 7$
366.3					$29/2^- \rightarrow 25/2^-$	$6 \rightarrow$
370.1		−0.09(7)	0.80(8)	$M1/E2$	$43/2^{(-)} \rightarrow 41/2^{(-)}$	$9 \rightarrow 10$
377.3		−0.06(6)	0.78(7)	$M1/E2$	$45/2^{(-)} \rightarrow 43/2^{(-)}$	$10 \rightarrow 9$
378.1	2.9				$13/2^- \rightarrow 9/2^-$	6
381.6					$33/2^- \rightarrow 33/2^+$	$1 \rightarrow 3$
401.1					$47/2^{(-)} \rightarrow 37/2^{(-)}$	$9 \rightarrow 10$
401.1					$49/2^{(-)} \rightarrow 47/2^{(-)}$	$10 \rightarrow 9$
403.2					$43/2^- \rightarrow 41/2^-$	$2 \rightarrow 1$
404.5	3.5	0.18(2)	1.14(2)	$E2$	$25/2^- \rightarrow 21/2^-$	1
414.3	96.4	0.26(1)	1.29(2)	$E2$	$21/2^+ \rightarrow 17/2^+$	3
418.9					$31/2^{(-)} \rightarrow 27/2^{(-)}$	9
421.8					$19/2^{(-)} \rightarrow (15/2^-)$	7
422.1		0.19(4)	1.44(6)	$E2$	$25/2^+ \rightarrow 21/2^+$	4
427.9					$51/2^{(-)} \rightarrow 49/2^{(-)}$	$9 \rightarrow 10$
429.2			0.82(5)	$E1$	$47/2^- \rightarrow 45/2^+$	$2 \rightarrow 3$
436.1	1.9				$25/3^- \rightarrow 21/2^-$	$1 \rightarrow 6$
441.2		0.03(3)	0.96(3)	$E1$	$43/2^- \rightarrow 41/2^+$	$2 \rightarrow 3$
450.8		−0.27(5)	0.69(7)	$E1$	$51/2^- \rightarrow 49/2^+$	$2 \rightarrow 3$
453.9	2.0		1.13(6)	$E2$	$31/2^- \rightarrow 27/2^-$	2
467.6		−0.19(4)	0.58(4)	$E1$	$55/2^- \rightarrow 53/2^+$	$2 \rightarrow 3$
468.7					$59/2^- \rightarrow 57/2^-$	$2 \rightarrow 1$
473.7			0.78(9)	$M1/E2$	$47/2^- \rightarrow 45/2^-$	$2 \rightarrow 1$
478.3	17.9	0.28(1)	1.34(1)	$E2$	$29/2^- \rightarrow 25/2^-$	1
481.5			0.92(11)	$M1/E2$	$55/2^- \rightarrow 53/2^-$	$2 \rightarrow 1$

TABLE I. (*Continued*.)

E_γ (keV)[a]	I_γ[b]	A_2[c]	R[d]	Mult.	Assignment	Band
486.2					$33/2^{(-)} \rightarrow 29/2^{(-)}$	10
489.2	1.2	−0.34(6)	0.64(5)	$M1/E2$	$21/2^- \rightarrow 19/2^{(-)}$	$1 \rightarrow 7$
492.6					$29/2^- \rightarrow 25/2^-$	6
500.9					$51/2^- \rightarrow 49/2^-$	$2 \rightarrow 1$
513.1	1.6				$17/2^- \rightarrow 13/2^-$	6
513.6	32.5	0.19(1)	1.20(1)	$E2$	$33/2^- \rightarrow 29/2^-$	1
514.5					$63/2^- \rightarrow 61/2^-$	$2 \rightarrow 1$
514.5	3.9	0.12(2)	1.18(2)	$E2$	$29/2^+ \rightarrow 25/2^+$	4
521.2					$25/2^+ \rightarrow 25/2^+$	$4 \rightarrow 3$
527.1	91.2	0.12(1)	1.23(1)	$E2$	$25/2^+ \rightarrow 21/2^+$	3
528.5	2.2				$39/2^- \rightarrow 37/2^+$	$2 \rightarrow 3$
530.3					$(33/2^-) \rightarrow (29/2^-)$	5
533.5	1.2				$23/2^{(-)} \rightarrow 19/2^{(-)}$	7
536.2	8.1	0.50(2)	1.21(3)	$E2$	$35/2^- \rightarrow 31/2^-$	2
544.2					$(33/2^-) \rightarrow 29/2^-$	6
545.8					$35/2^{(-)} \rightarrow 31/2^{(-)}$	9
556.8					$35/2^{(-)} \rightarrow (31/2^-)$	8
570.8	5.9				$29/2^- \rightarrow 29/2^+$	$1 \rightarrow 3$
574.3	30.4	0.35(2)	1.38(1)	$E2$	$37/2^- \rightarrow 33/2^-$	1
592.2					$37/2^{(-)} \rightarrow 33/2^{(-)}$	10
592.5					$(29/2^-) \rightarrow 25/2^-$	$5 \rightarrow 6$
592.5	3.3				$21/2^- \rightarrow 17/2^-$	6
601.2	6.3	−0.02(2)	0.95(3)	$(E2)$	$33/2^+ \rightarrow 29/2^+$	4
607.1	2.7				$27/2^{(-)} \rightarrow 23/2^{(-)}$	7
612.9					$(37/2^-) \rightarrow (33/2^-)$	6
618.3					$(37/2^-) \rightarrow (33/2^-)$	5
621.7	67.7	0.24(1)	1.34(2)	$E2$	$29/2^+ \rightarrow 25/2^+$	3
624.9	1.0				$21/2^- \rightarrow 17/2^-$	$1 \rightarrow 6$
627.4					$21/2^+ \rightarrow 21/2^+$	$4 \rightarrow 3$
629.3	12.7	0.37(1)	1.42(3)	$E2$	$39/2^- \rightarrow 35/2^-$	2
632.8	2.1		1.24(11)	$E2$	$39/2^{(-)} \rightarrow 35/2^{(-)}$	8
633.8					$25/2^- \rightarrow 21/2^-$	6
639.5		0.29(2)	1.47(35)	$E2$	$39/2^{(-)} \rightarrow 35/2^{(-)}$	9
650.9	36.8	0.33(1)	1.35(1)	$E2$	$41/2^- \rightarrow 37/2^-$	1
664.4	9.5	−0.32(2)	0.70(1)	$E1$	$35/2^- \rightarrow 33/2^+$	$2 \rightarrow 3$
676.2					$(41/2^-) \rightarrow (37/2^-)$	6
678.6	8.3	0.26(2)	1.43(13)	$E2$	$37/2^+ \rightarrow 33/2^+$	4
679.3					$41/2^{(-)} \rightarrow 37/2^{(-)}$	10
695.7					$(17/2^+) \rightarrow 17/2^+$	$4 \rightarrow 3$
702.8	48.1	0.31(1)	1.34(2)	$E2$	$33/2^+ \rightarrow 29/2^+$	3
703.7					$(41/2^-) \rightarrow (37/2^-)$	5
705.3	1.8				$43/2^{(-)} \rightarrow 39/2^{(-)}$	8
714.2	6.8				$25/2^- \rightarrow 25/2^+$	$1 \rightarrow 3$
715.4	20.2	0.34(2)	1.32(1)	$E2$	$43/2^- \rightarrow 39/2^-$	2
718.0					$43/2^{(-)} \rightarrow 39/2^{(-)}$	9
727.5	36.1	0.37(2)	1.42(1)	$E2$	$45/2^- \rightarrow 41/2^-$	1
737.9	5.8	0.34(3)	1.37(4)	$E2$	$41/2^+ \rightarrow 37/2^+$	4
747.7					$45/2^{(-)} \rightarrow 41/2^{(-)}$	10
750.3	3.3	0.26(3)	1.32(3)	$E2$	$45/2^+ \rightarrow 31/2^+$	4
751.2					$(45/2^-) \rightarrow (41/2^-)$	6
761.2					$25/2^- \rightarrow 21/2^-$	$\rightarrow 6$
761.3					$19/2^{(-)} \rightarrow 17/2^+$	$7 \rightarrow 3$
764.9	39.9	0.31(1)	1.21(2)	$E2$	$37/2^+ \rightarrow 33/2^+$	3
778.3		0.31(2)	1.53(14)	$E2$	$47/2^{(-)} \rightarrow 43/2^{(-)}$	9
780.7	2.5		1.24(7)	$E2$	$47/2^{(-)} \rightarrow 43/2^{-)}$	8
782.1	5.1	0.31(2)	1.15(3)	$E2$	$49/2^+ \rightarrow 45/2^+$	4
789.7	13.1	0.32(1)	1.28(1)	$E2$	$59/2^- \rightarrow 55/2^-$	2

TABLE I. (*Continued*.)

E_γ (keV)[a]	I_γ[b]	A_2[c]	R[d]	Mult.	Assignment	Band
791.6	35.1	0.19(1)	1.34(2)	$E2$	$53/2^+ \rightarrow 49/2^+$	3
791.9	21.1	0.26(1)	1.30(1)	$E2$	$61/2^- \rightarrow 57/2^-$	1
797.9	17.2		1.27(2)	$E2$	$47/2^- \rightarrow 43/2^-$	2
800.3	37.0	0.30(1)	1.34(3)	$E2$	$49/2^- \rightarrow 45/2^-$	1
802.5					$49/2^{(-)} \rightarrow 45/2^{(-)}$	10
802.7					$(49/2^-) \rightarrow (45/2^-)$	6
803.0	51.3		1.35(1)	$E2$	$41/2^+ \rightarrow 37/2^+$	3
803.5	20.8	0.30(1)	1.34(3)	$E2$	$57/2^- \rightarrow 53/2^-$	1
806.2	47.4		1.29(2)	$E2$	$49/2^+ \rightarrow 45/2^+$	3
809.1	13.2	0.38(2)	1.25(1)	$E2$	$55/2^- \rightarrow 51/2^-$	2
809.6	47.4		1.29(2)	$E2$	$45/2^+ \rightarrow 41/2^+$	3
817.3					$(59/2^-) \rightarrow (55/2^-)$	8
827.8					$(55/2^-) \rightarrow (51/2^-)$	8
828.2					$51/2^{(-)} \rightarrow 47/2^{(-)}$	9
829.2	36.8	0.26(1)	1.24(2)	$E2$	$51/2^- \rightarrow 47/2^-$	2
829.5	35.4	0.30(1)	1.26(1)	$E2$	$53/2^- \rightarrow 49/2^-$	1
830.8	8.0				$31/2^- \rightarrow 29/2^+$	$2 \rightarrow 3$
833.3	27.4	0.23(1)	1.33(2)	$E2$	$57/2^+ \rightarrow 53/2^+$	3
834.2					$39/2^{(-)} \rightarrow 37/2^+$	$8 \rightarrow 3$
837.1	2.6	−0.15(2)	1.15(4)	$E1$	$21/2^- \rightarrow 21/2^+$	$1 \rightarrow 3$
838.7	10.6	0.19(1)	1.24(1)	$E2$	$63/2^- \rightarrow 59/2^-$	2
844.3					$(53/2^-) \rightarrow (49/2^-)$	6
845.9	1.0				$51/2^{(-)} \rightarrow 47/2^{(-)}$	8
846.2					$53/2^{(-)} \rightarrow 49/2^{(-)}$	10
855.8	1.9	0.44(3)	1.35(8)	$E2$	$53/2^+ \rightarrow 49/2^+$	4
867.9	9.9	0.41(2)	1.47(1)	$E2$	$67/2^- \rightarrow 63/2^-$	2
874.7	20.8	0.40(1)	1.40(1)	$E2$	$65/2^- \rightarrow 61/2^-$	1
879.2					$23/2^{(-)} \rightarrow 21/2^+$	$7 \rightarrow 3$
883.2	4.0	0.58(4)	1.45(5)	$E2$	$49/2^+ \rightarrow 45/2^+$	$4 \rightarrow 3$
905.6					$57/2^{(-)} \rightarrow 53/2^{(-)}$	10
914.9	16.3	0.34(2)	1.22(3)	$E2$	$61/2^+ \rightarrow 57/2^+$	3
924.5	2.3	0.44(2)	1.65(3)	$E2$	$61/2^+ \rightarrow 57/2^+$	4
924.5	2.3	0.44(2)	1.65(3)	$E2$	$65/2^+ \rightarrow 61/2^+$	4
932.7					$53/2^+ \rightarrow 49/2^+$	$4 \rightarrow 3$
956.9	14.8	0.44(2)	1.31(4)	$E2$	$65/2^+ \rightarrow 61/2^+$	3
960.5	2.0				$27/2^{(-)} \rightarrow 25/2^+$	$7 \rightarrow 3$
961.7					$17/2^+ \rightarrow 13/2^+$	$4 \rightarrow 3$
966.9	2.1		0.79(9)	$(E1)$	$35/2^{(-)} \rightarrow 33/2^+$	$8 \rightarrow 3$
969.8		0.34(6)	1.31(7)	$E2$	$57/2^+ \rightarrow 53/2^+$	4
991.3					$37/2^+ \rightarrow 33/2^+$	$4 \rightarrow 3$
998.7	1.2	−0.23(2)	0.47(3)	$E1$	$27/2^- \rightarrow 25/2^+$	$2 \rightarrow 3$
1014.6	1.3	0.16(5)	1.48(5)	$E2$	$33/2^+ \rightarrow 29/2^+$	$4 \rightarrow 3$
1036.7	2.9	0.19(4)	1.36(4)	$E2$	$29/2^+ \rightarrow 25/2^+$	$4 \rightarrow 3$
1038.5					$25/2^- \rightarrow 25/2^+$	$\rightarrow 3$
1040.8	1.2				$21/2^+ \rightarrow 17/2^+$	$4 \rightarrow 3$
1048.1	2.1	0.05(5)	1.42(6)	$E2$	$25/2^+ \rightarrow 21/2^+$	$4 \rightarrow 3$
1111.8			0.74(11)	$(E1)$	$31/2^{(-)} \rightarrow 29/2^+$	$8 \rightarrow 3$
1236.0		−0.25(8)	0.84(7)	$(E1)$	$31/2^{(-)} \rightarrow 29/2^+$	$9 \rightarrow 3$
1264.9					$(31/2^-) \rightarrow 29/2^+$	$\rightarrow 3$
1440.1			0.89(14)	$(E1)$	$27/2^{(-)} \rightarrow 25/2^+$	$9 \rightarrow 3$
1710.9					$31/2^{(-)} \rightarrow 29/2^+$	$9 \rightarrow 3$

[a]The γ-ray energies are estimated to be accurate to ± 0.3 keV for the strong transitions ($I_\gamma > 10$), rising to ± 0.6 keV for the weaker transitions.
[b]Intensities not listed are less than 1% of the 266 keV ($17/2^+ \rightarrow 13/2^+$) transition. Errors on the intensities are estimated to be less than 5% of the quoted values for strong transitions ($I_\gamma > 10$) and less than 10% for the weaker transitions.
[c]$\gamma\gamma$-gated coefficients.
[d]$\gamma\gamma\gamma\gamma$-gated angular-intensity ratios.

TABLE II. Energies, intensities and angular-distribution data for the transitions assigned to ^{157}Er which are shown in Fig. 3.

E_γ (keV)[a]	I_γ[b]	A_2[c]	R[d]	Mult.	Assignment	Band
277.6		−0.36(4)	0.77(2)	$M1/E2$	$83/2^- \rightarrow 81/2^-$	$2 \rightarrow 1$
315.4			0.85(7)	$M1/E2$	$77/2^- \rightarrow 75/2^-$	$1 \rightarrow 2$
450.3		−0.27(5)	0.69(7)	$M1/E2$	$75/2^- \rightarrow 73/2^-$	$2 \rightarrow 1$
597.1	4.6	−0.27(3)	0.95(1)	$M1/E2$	$71/2^+ \rightarrow 69/2^+$	$\rightarrow 3$
601.2					$\rightarrow 71/2^+$	$\rightarrow 3$
650.2	4.1	0.34(1)	1.38(1)	$E2$	$87/2^- \rightarrow 83/2^-$	2
671.1	1.7	−0.87(2)	0.31(1)	$M1/E2$	$79/2^- \rightarrow 77/2^-$	$2 \rightarrow 1$
722.4	1.0	0.33(2)	1.58(5)	$E2$	$77/2^- \rightarrow 73/2^-$	$1 \rightarrow$
753.9	1.0	0.60(4)	1.44(6)	$E2$	$93/2^+ \rightarrow 89/2^+$	3
764.1	2.1	0.35(1)	1.37(2)	$E2$	$77/2^- \rightarrow 73/2^-$	1
770.4				$E2$	$89/2^+ \rightarrow 85/2^+$	3
813.9	1.1	0.58(4)	1.27(4)	$E2$	$89/2^- \rightarrow 85/2^-$	1
833.3	27.4	0.23(1)	1.33(2)	$E2$	$69/2^+ \rightarrow 65/2^+$	3
859.4	3.9	0.82(6)	1.29(9)	$E2$	$77/2^+ \rightarrow 73/2^+$	3
892.0					$(75/2^+) \rightarrow 71/2^+$	$\rightarrow 3$
892.7	8.5	0.37(2)	1.31(4)	$E2$	$81/2^+ \rightarrow 77/2^+$	3
894.7	7.7	0.28(1)	1.34(2)	$E2$	$71/2^- \rightarrow 67/2^-$	2
907.2					$\rightarrow 89/2^-$	$\rightarrow 2$
920.3	1.1	0.38(2)	1.43(2)	$E2$	$85/2^- \rightarrow 81/2^-$	1
923.7	3.6	0.36(2)	1.51(1)	$E2$	$83/2^- \rightarrow 79/2^-$	2
938.9	4.9	0.33(2)	1.33(1)	$E2$	$75/2^- \rightarrow 71/2^-$	2
940.3	2.2	0.37(2)	1.42(1)	$E2$	$73/2^- \rightarrow 69/2^-$	1
952.9	5.0	0.34(2)	1.31(1)	$E2$	$69/2^- \rightarrow 65/2^-$	1
982.3	2.0	0.28(2)	1.25(2)	$E2$	$73/2^- \rightarrow 69/2^-$	$\rightarrow 1$
985.7	3.5	0.25(2)	1.29(2)	$E2$	$79/2^- \rightarrow 75/2^-$	2
1017.4		−0.28(3)	0.79(4)	$E1$	$89/2^+ \rightarrow 87/2^-$	$3 \rightarrow 2$
1032.7	1.9				$\rightarrow 73/2^+$	$\rightarrow 3$
1038.1					$(79/2^+) \rightarrow 75/2^+$	$\rightarrow 3$
1045.5					$\rightarrow 91/2^-$	$\rightarrow 2$
1049.0					$\rightarrow 79/2^-$	$\rightarrow 2$
1071.6		0.38(6)	1.39(8)	$E2$	$75/2^+ \rightarrow 71/2^+$	$\rightarrow 3$
1079.1	4.4	0.39(3)	1.37(4)	$E2$	$73/2^+ \rightarrow 69/2^+$	3
1083.4					$\rightarrow 89/2^-$	$\rightarrow 2$
1111.6		0.39(7)	1.24(10)	$E2$	$73/2^+ \rightarrow 69/2^+$	$\rightarrow 3$
1125.6		0.23(4)	1.42(5)	$E2$	$77/2^- \rightarrow 73/2^-$	$\rightarrow 1$
1232.8		0.8(1)	1.30(10)	$E2$	$81/2^- \rightarrow 77/2^-$	$\rightarrow 1$
1233.8					$\rightarrow 71/2^+$	$\rightarrow 3$
1234.4		0.49(8)	1.40(10)	$E2$	$85/2^+ \rightarrow 81/2^+$	3
1264.3		0.0(6)	0.84(6)	$M1/E2$	$89/2^- \rightarrow 87/2^-$	$\rightarrow 2$
1293.2					$\rightarrow 73/2^-$	$\rightarrow 1$
1316.3	1.2	0.32(2)	1.36(3)	$E2$	$81/2^- \rightarrow 77/2^-$	1
1378.3		0.31(1)	1.58(16)	$E2$	$79/2^- \rightarrow 75/2^-$	$\rightarrow 2$
1387.1					$\rightarrow 73/2^-$	$\rightarrow 1$
1420.6					$\rightarrow 89/2^-$	$\rightarrow 1$
1433.1					$\rightarrow 91/2^-$	$\rightarrow 2$
1439.1			2.36(15)	$M1/E2$	$89/2^- \rightarrow 87/2^-$	$\rightarrow 2$
1452.8			1.31(17)	$E2$	$85/2^+ \rightarrow 81/2^+$	$\rightarrow 3$
1480.2			0.89(20)	$M1/E2$	$95/2^+ \rightarrow 93/2^+$	$\rightarrow 3$
1494.7					$\rightarrow 89/2^-$	$\rightarrow 1$
(1499.7)					$\rightarrow 91/2^-$	$\rightarrow 2$
1538.4			1.75(24)	$M1/E2$	$89/2^- \rightarrow 87/2^-$	$\rightarrow 2$
1556.3			1.38(44)	$E2$	$93/2^- \rightarrow 89/2^-$	$\rightarrow 1$
1581.6			1.22(13)	$E2$	$91/2^- \rightarrow 87/2^-$	$\rightarrow 2$
1635.7					$\rightarrow 93/2^+$	$\rightarrow 3$
1695.2					$\rightarrow 93/2^+$	$\rightarrow 3$
1701.0					$\rightarrow 93/2^+$	$\rightarrow 3$
1706.4			1.49(17)	$E2$	$93/2^- \rightarrow 89/2^-$	$\rightarrow 1$

TABLE II. (*Continued*.)

E_γ (keV)[a]	I_γ[b]	A_2[c]	R[d]	Mult.	Assignment	Band
1714.8					$\rightarrow 87/2^-$	$\rightarrow 2$
1780.2					$\rightarrow 87/2^-$	$\rightarrow 2$
1914.9			1.41(23)	$E2$	$91/2^- \rightarrow 87/2^-$	$\rightarrow 2$
2075.1			1.45(11)	$E2$	$91/2^- \rightarrow 87/2^-$	$\rightarrow 2$
2102.6			1.48(14)	$E2$	$93/2^- \rightarrow 89/2^-$	$\rightarrow 1$
2125.4					$\rightarrow 93/2^+$	$\rightarrow 3$
2138.8			1.46(13)	$E2$	$91/2^- \rightarrow 87/2^-$	$\rightarrow 2$
(2166)					$\rightarrow 89/2^-$	$\rightarrow 2$
2204.5					$\rightarrow 95/2^+$	$\rightarrow 3$
2408.7					$\rightarrow 87/2^-$	$\rightarrow 2$

[a]The γ-ray energies are estimated to be accurate to ± 0.3 keV for the strong transitions ($I_\gamma > 10$), rising to ± 0.6 keV for the weaker transitions.
[b]Intensities not listed are less than 1% of the 266 keV ($17/2^+ \rightarrow 13/2^+$) transition of Band 3. Errors on the intensities are estimated to be less than 5% of the quoted values for strong transitions ($I_\gamma > 10$) and less than 10% for the weaker transitions.
[c]$\gamma\gamma$-gated angular-distribution coefficients.
[d]$\gamma\gamma\gamma\gamma$-gated angular-intensity ratios.

3. Bands 5 and 6

Reevaluation of the previous work [7] by Brown *et al*. [17] placed the 513 keV transition in the negative-parity Band 6. This band was then established as built on the $I^\pi = 5/2^-$ ground state of ^{157}Er through comparison with the ^{153}Gd isotone [17]. Similar bands to Band 6 in ^{157}Er are also observed in the ^{155}Dy isotone [18] and the ^{159}Er isotope [19]. The present work confirms this placement and has extended Band 6 to

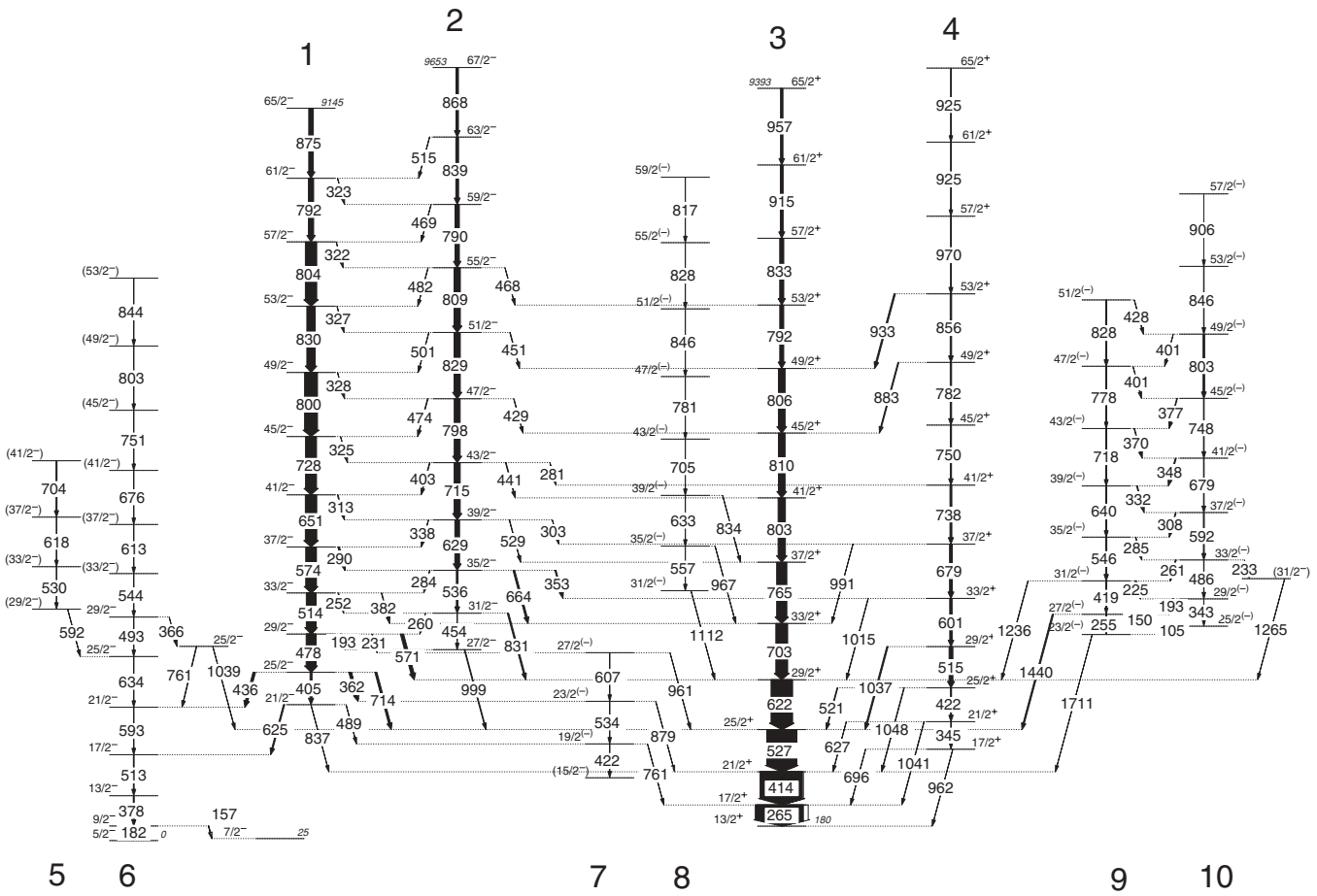

FIG. 2. Low-spin section of the ^{157}Er level scheme showing γ-ray transitions below spin $67/2$. Energies are labeled in keV and the widths of the arrows are proportional to the transition intensities. The properties of the transitions are listed in Table I.

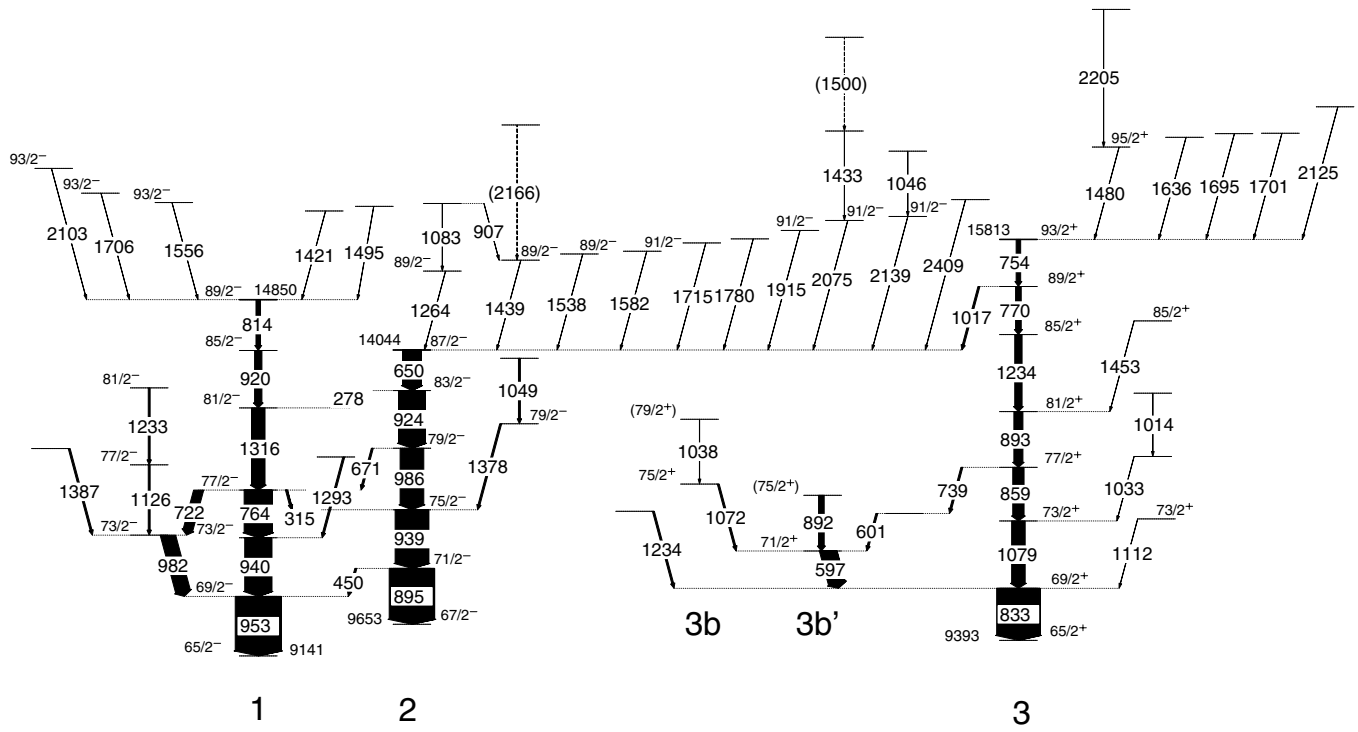

FIG. 3. High-spin section of the ^{157}Er level scheme showing γ-ray transitions above spin 65/2. Energies are labeled in keV and the widths of the arrows are proportional to the transition intensities.The properties of the transitions are listed in Table II.

higher spin with the addition of the 844 keV transition. Band 5 is a new sequence of three γ rays which decays into Band 6 at $I^\pi = 25/2^-$ via the 592 keV transition. These transitions are assumed to be of $E2$ character in Fig. 2.

4. Bands 7 and 8

The sequence of two transitions in Band 7 [7] has been confirmed and the sequence extended to lower spin with the addition of a 422 keV transition of assumed $E2$ character. However no decay could be established from the $I^\pi = (15/2^-)$ band head of Band 7.

Band 8 is a newly established sequence of seven transitions from $I^\pi = 31/2^{(-)}$ up to $59/2^{(-)}$; a spectrum is shown in Fig. 5. This band decays into the positive-parity Band 3 via the 1112, 967, and 834 keV transitions. Measured angular-intensity ratios for the 633 and 781 keV inband transitions confirm their quadrupole nature, while measurements for the 967 and 1112 keV linking transitions are consistent with dipole character (assumed $E1$).

5. Strongly coupled bands 9 and 10

Bands 9 and 10 represent a strongly coupled band structure which was established in the previous work [7]. It has been possible to extract angular-distribution coefficients for several of the interconnecting $\Delta I = 1$ transitions. The values (see

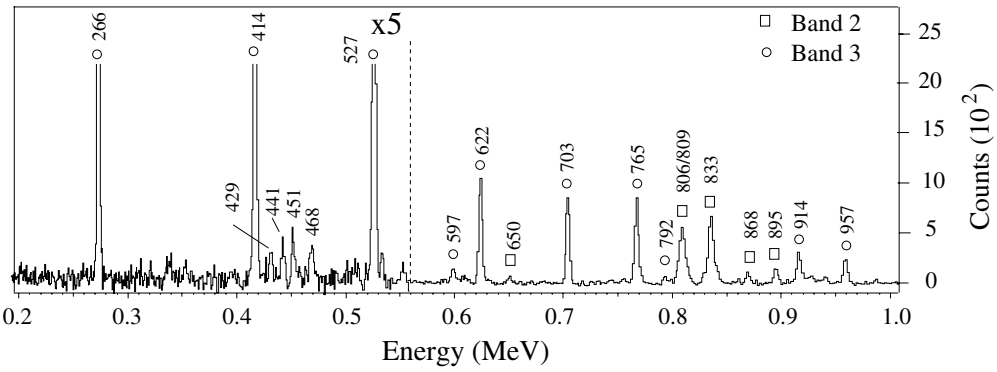

FIG. 4. Single triple-gated ($x = 790$, $y = 810$, $z = 803$ keV) γ^4 coincidence spectrum generated from the hypercube. The lower energy portion (< 0.56 MeV) of the spectrum has been magnified to illustrate the newly observed 429, 451, and 468 keV γ rays decaying from Band 2 into Band 3.

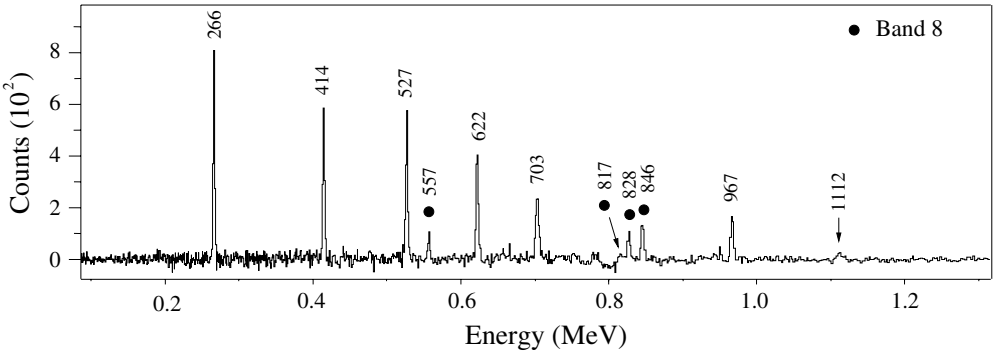

FIG. 5. Single triple-gated ($x = 781$, $y = 705$, $z = 633$ keV) γ^4 coincidence spectrum set on three transitions of Band 8. The other four members of Band 8 are denoted and the 967 and 1112 keV transitions linking Band 8 to Band 3 are clearly evident.

Table I) tend to be less negative than expected for pure $\Delta I = 1$ transitions and strongly suggest that the transitions are of mixed $M1/E2$ character with positive $E2/M1$ multipole-mixing ratios δ. The $E2$ inband transitions of Bands 9 and 10 are considerably weaker than the interconnecting $\Delta I = 1$ transitions.

This strongly coupled structure was previously observed to decay to Band 3 via 1236, 1440 and 1711 keV transitions [7] (see Fig. 6). A further transition of energy 1265 keV has now been observed which decays from Band 10 into the $29/2^+$ state of Band 3. Angular-intensity ratios extracted for the 1236 and 1440 keV transitions imply $\Delta I = 1$ character.

B. High-spin results

The high-spin section of the level scheme of ^{157}Er is shown in Fig. 3. The two negative-parity Bands 1 and 2 were previously established up to the terminating states at $I^\pi = 89/2^-$ and $87/2^-$, respectively [7]. A third band-terminating state has now been established in the positive-parity Band 3 at $I^\pi = 93/2^+$, and a multitude of high-energy transitions of weak intensity has been identified feeding the three terminating states, most of which are reported in Ref. [11].

1. Band 1

Five high-energy transitions have been observed feeding into the $89/2^-$ terminating state of Band 1, as shown in the γ-ray spectrum of Fig. 7; the high-energy, low-intensity γ rays can be seen in the 1.4−2.1 MeV region. The measured properties of the transitions feeding into the terminating state are presented in Table II. Three of the transitions could be identified with $\Delta I = 2$ ($E2$) character through angular-intensity ratio measurements. Only ≈41% of the total intensity feeding into the $89/2^-$ state is accounted for.

Band 1 branches above the $69/2^-$ state, yielding two $73/2^-$ states. The 1126 keV γ ray tentatively suggested previously [7] to be an $E2$ transition feeding the higher $73/2^-$ state is confirmed in the present work. Moreover, a 1233 keV γ ray of quadrupole nature has been placed above this transition.

2. Band 2

The present work has identified ten high-energy transitions which feed the $I^\pi = 87/2^-$ band-terminating state of Band 2. The measured properties of these high-energy γ rays are summarized in Table II. The stronger γ rays have been fitted to an angular-distribution function, but for several of the

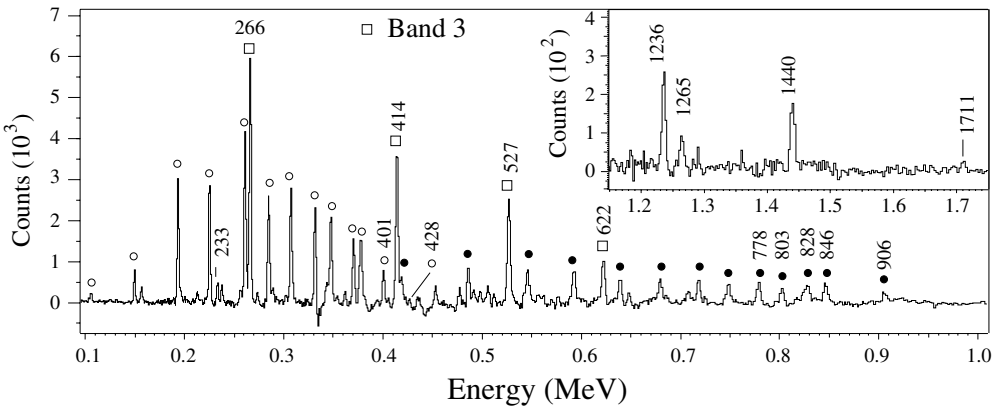

FIG. 6. Triple-gated γ^4 coincidence spectrum of γ rays in coincidence with the 285, 307, 332, 347, 370, 377 keV transitions connecting Bands 9 and 10. These strong interconnecting dipole transitions have been labeled with an open circle, and the inband transitions of Bands 9 and 10 with a filled circle. The inset shows the high-energy transitions linking this strongly coupled structure to Band 3.

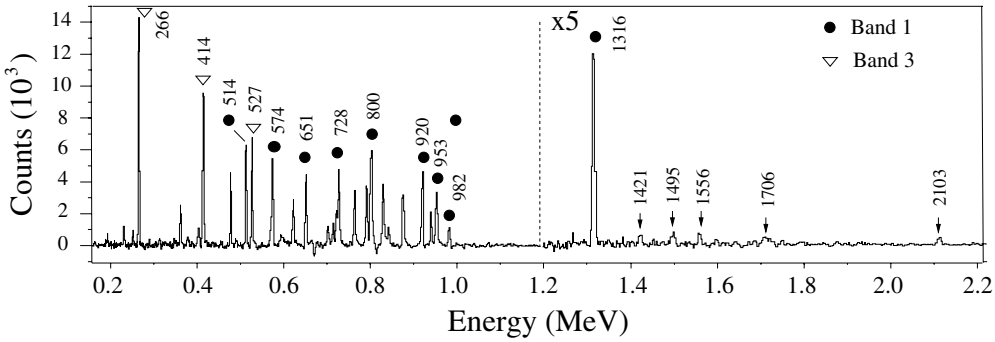

FIG. 7. Triple-gated γ^4 coincidence spectrum of γ rays in coincidence with the 814 keV transition against a gate file containing a list of γ rays in Band 1 (x = 814 keV, $y = z$ = gate file). The main peaks are labeled by symbols corresponding to their associated band. Above 1.2 MeV the high-energy transitions feeding into the $89/2^-$ state of Band 1 are labeled.

weaker transitions only an angular-intensity ratio could be extracted.

Approximately 33% of the total feeding intensity is accounted for. In addition, an $E1$ transition of energy 1017 keV decays from the $89/2^+$ state of Band 3, accounting for a further 22% of the feeding intensity. A γ^3 coincidence spectrum is shown in Fig. 8 and clearly shows the low-intensity transitions in the 1.0−2.5 MeV region. Angular-intensity ratios for the 1264, 1439, and 1538 keV transitions feeding into the $87/2^-$ terminating state of Band 2 suggest mixed $M1/E2\ \Delta I = 1$ character. The A_2 angular-distribution coefficient for the 1264 keV transition is close to zero, implying a positive $E2/M1$ multipole-mixing ratio. In contrast, the 1439 and 1538 keV transitions have angular-intensity ratios larger than typical for stretched $\Delta I = 2$ transitions; this can be explained by mixed $M1/E2\ \Delta I = 1$ character for these transitions with large positive $E2/M1$ multipole-mixing ratios.

From the remaining seven transitions, it was possible to identify three of them with $\Delta I = 2$ ($E2$) character. Several of the stronger transitions have been observed in coincidence with transitions from higher levels. The spectrum of Fig. 9 shows transitions in coincidence with the 1264 keV γ ray gated against a list containing members of Band 2. A transition of energy 1083 keV is clearly visible in this spectrum and feeds in through the 1264 keV γ ray. Other transitions of energies (2166), 1433, (1500), and 1046 keV are placed above some of the direct feeders of the $87/2^-$ state (see Fig. 3). The state decaying by the 1083 keV transition also decays through the 1439 keV transition via a 907 keV transition.

The $75/2^-$ state in Band 2 is fed by a second transition at energy 1378 keV. This γ ray has been assigned an $E2$ transition based on angular-intensity ratio measurement. A further γ ray of energy 1049 keV is placed above the 1378 keV transition.

A 450 keV γ ray has been observed decaying from $71/2^-$ state of Band 2 into the $69/2^-$ state of Band 1. This is in addition to the 278 ($83/2^- \rightarrow 81/2^-$), and 671 keV ($79/2^- \rightarrow 77/2^-$) transitions established in the previous work [7]. The 671 keV transition has a large negative A_2 coefficient (−0.87) indicating a mixed $M1/E2$ transition with a large negative $E2/M1$ multipole-mixing ratio. This is in contrast to the 278 keV transition which has a much smaller A_2 value (−0.36) consistent with a small negative multipole-mixing ratio.

3. Band 3

Band 3 was previously established up to the $I^\pi = 85/2^+$ state [7] but has now been extended with the addition of two new γ rays of energy 770 and 754 keV. The 754 keV ($93/2^+ \rightarrow 89/2^+$) transition has an angular-distribution

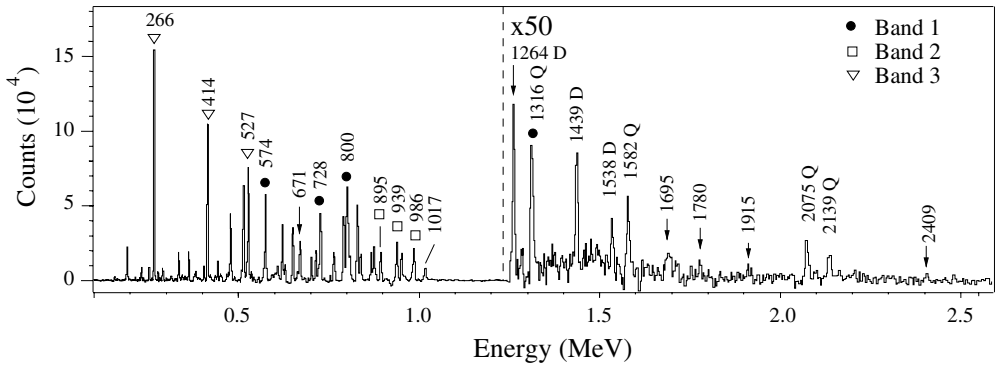

FIG. 8. Double-gated γ^3 coincidence spectrum of γ rays in coincidence with the 650 and 924 keV transitions in Band 2. Note the large multiplication in the scale needed above 1 MeV in order to illustrate the many weak feeding transitions. Above 1 MeV, $\Delta I = 1$ transitions are labeled by 'D' (dipole) and $\Delta I = 2$ transitions by 'Q' (quadrupole).

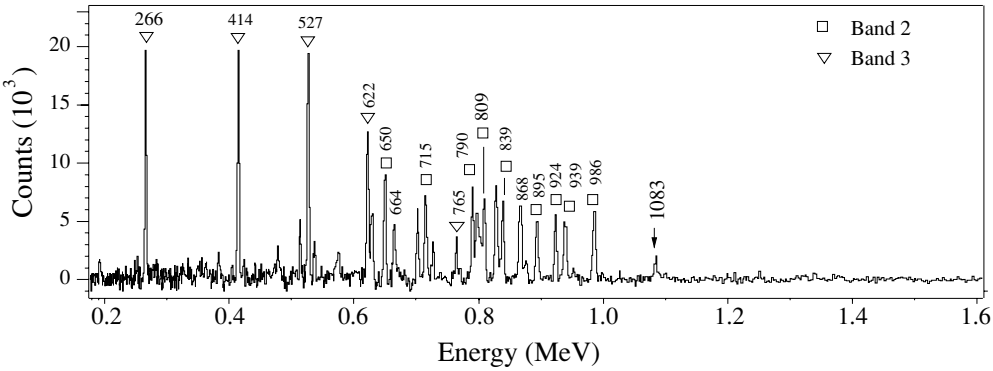

FIG. 9. Triple-gated γ^4 coincidence spectrum of γ rays in coincidence with 1264 keV transition gated against a list of γ-rays in Band 2 ($x = 1264$ keV, $y = z =$ gate file). The 1083 keV γ-ray is clearly seen in the spectrum.

coefficient consistent with $\Delta I = 2$ ($E2$) character. It was not possible for a direct measurement of the multipolarity of the 770 keV transition; however the $89/2^+$ state is firmly established by the observation of the 1017 keV $E1$ transition decaying from Band 3 into the $87/2^-$ terminating state of Band 2.

Five high-energy transitions have been observed (see Fig. 10) feeding into the newly established $93/2^+$ terminating state accounting for approximately 58% of the feeding intensity. The measured properties of the high-energy feeding transitions are summarized in Table II. The strongest of these feeding transitions, of energy 1480 keV, has an angular-intensity ratio consistent with a mixed $M1/E2$ $\Delta I = 1$ character. A 2205 keV γ ray is placed above the 1480 keV transition.

The $81/2^+$ state of Band 3 is fed by a high-energy $\Delta I = 2$ ($E2$) 1453 keV γ ray. The 1033 keV γ ray has now been placed decaying into the $73/2^+$ state of Band 3 in contrast to the previous work [7], with a further 1014 keV transition placed above it. At spin $69/2^+$ the decay path fragments with transitions of 597, 1112, and 1294 keV feeding this state in addition to the inband 1079 keV transition. The present work has confirmed the dipole nature ($M1/E2$) of the 597 keV γ ray and the quadrupole nature of the 1072 keV γ ray. The $\Delta I = 2$ character of the 1112 keV transition is also confirmed.

III. DISCUSSION

The first part of this Section reviews the low-spin structures of ^{157}Er as shown in Fig. 2, while the second part discusses the high-spin properties related to Fig. 3.

A. Low-spin structures

The configuration assignments of the bands in ^{157}Er are listed in Table III and discussed in detail below.

1. The $\Delta I = 2$ Bands 1–8

Configurations of the rotational bands in ^{157}Er have been discussed previously in Ref. [7] and more recently in Ref. [17] for the case of Band 6. The neutron Fermi level lies between the $[660]1/2^+$ and $[651]3/2^+ N_{\rm osc} = 6$ ($\nu i_{13/2}$) intruder orbitals and close to the $N_{\rm osc} = 5$ $[521]3/2^-$ and $[523]5/2^-$ ($\nu f_{7/2}/h_{9/2}$) orbitals. The relevant high-j orbitals near the proton Fermi surface are the $[523]7/2^-$ ($\pi h_{11/2}$) and $[404]7/2^+$ ($\pi g_{7/2}$) orbitals. The strongly populated positive-parity Band 3 is yrast at low spin and is associated with the $[651]3/2^+$ orbital. The bands shown to the left of Band 3 in Fig. 2, including the newly identified Band 8, may be associated with the negative-parity orbitals. Bands 1 and 2 form signature

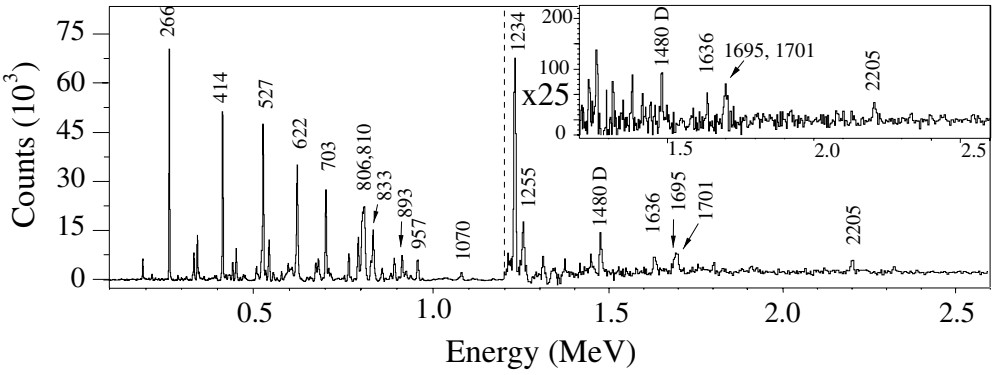

FIG. 10. Triple-gated γ^4 coincidence spectrum produced from the sum of triple gates on the 754 keV transition in coincidence with a gatelist of γ rays in Band 2 ($x = 754$ keV, $y = z =$ gate file). The inset shows high-energy γ rays in coincidence with the 754 keV transition gated against a gate file containing members of Band 3 ($x = 754$ keV, $y = z =$ gate file).

TABLE III. Quasiparticle configurations assigned to the bands of ^{157}Er as shown in Fig. 2. The configurations are labeled by their dominant Nilsson components. Alignments of $i_{13/2}$ quasineutrons are explicitly shown, while at high spin $h_{11/2}$ quasiproton alignments are also observed in some bands.

Band No.	(Parity, signature)	Configuration
Band 1	$(-,+1/2)$	$\nu[523]5/2^- \otimes (\nu i_{13/2})^2$
Band 2	$(-,-1/2)$	$\nu[523]5/2^- \otimes (\nu i_{13/2})^2$
Band 3	$(+,+1/2)$	$\nu[651]3/2^+ \rightarrow \nu[651]3/2^+ \otimes (\nu i_{13/2})^2$
Band 4	$(+,+1/2)$	$\nu[651]3/2^+ \otimes \gamma$ vibration
Band 6	$(-,-1/2)$	$\nu[521]3/2^- \rightarrow \nu[521]3/2^- \otimes (\nu i_{13/2})^2$
Band 7	$(-,+1/2)$	$\nu[521]3/2^-$
Band 8	$(-,+1/2)$	$\nu[521]3/2^- \otimes (\nu i_{13/2})^2$
Band 9	$(-,-1/2)$	$\nu[651]3/2^+ \otimes \pi\{[523]7/2^- \otimes [404]7/2^+\}_{K=7}$
Band 10	$(-,+1/2)$	$\nu[651]3/2^+ \otimes \pi\{[523]7/2^- \otimes [404]7/2^+\}_{K=7}$

partners, while Bands 7 and 8 together may form the signature partner of Band 6. The alignment properties of the bands in ^{157}Er are shown in Fig. 11 and have been previously discussed in Ref [7]. Rotational alignments of pairs of $i_{13/2}$ quasineutrons are seen at frequencies $\omega \approx 0.28$ MeV/$\hbar$ and $\omega \approx 0.40$ MeV/$\hbar$. At higher frequencies there is also evidence for the rotational alignment of a pair of $h_{11/2}$ quasiprotons. Band 4, with the same parity and signature as Band 3, has been discussed in terms of a γ vibration coupled to the Band 3 structure $(\nu i_{13/2})$ [7].

2. *Strongly coupled bands 9 and 10*

Bands 9 and 10 together form a strongly coupled $\Delta I = 1$ structure where the odd $\nu i_{13/2}$ neutron is coupled to the high-K $\{[523]7/2^- \otimes [404]7/2^+\}_{K=7}$ 2-quasiproton structure [7]. The single $i_{13/2}$ neutron blocks the lowest $(\nu i_{13/2})^2$ alignment, seen at $\omega \approx 0.28$ MeV/$\hbar$ in Fig. 11. Similar high-K multiquasiparticle structures are seen in heavier erbium isotopes [20]. The large K-value of Bands 9/10 enhances the $M1$ strength, as can be seen in Fig. 12 which plots experimental $B(M1; I \rightarrow I-1)/B(E2; I \rightarrow I-2)$ ratios of reduced transition probabilities; the values average around 2.0 $\mu_N^2/(e\text{b})^2$. For comparison, experimental $B(M1)/B(E2)$ ratios are also shown for Bands 1/2 and are seen to be at least an order of magnitude smaller.

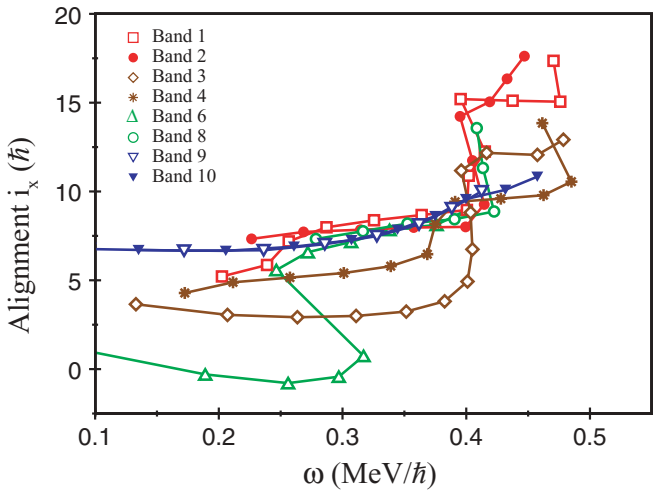

FIG. 11. (Color online) Experimental alignments for the bands in ^{157}Er. A reference with Harris parameters $\Im_0 = 32.1\hbar^2$ MeV^{-1} and $\Im_1 = 34.0\hbar^4$ MeV^{-3} has been subtracted.

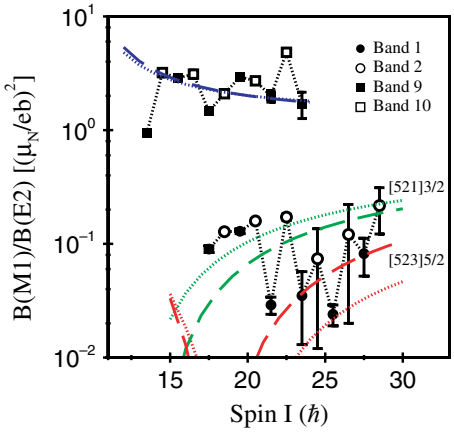

FIG. 12. (Color online) Experimental and theoretical $B(M1)/B(E2)$ ratios of reduced transition probabilities for Bands 1/2 and Bands 9/10 in ^{157}Er. Calculated values used either pure single-particle g-factors (dotted lines) or g-factors obtained from cranking calculations (dashed lines). For Bands 1/2 neutron orbitals $[521]3/2^-$ and $[523]5/2^-$ were considered.

Calculated $B(M1; I \rightarrow I-1)/B(E2; I \rightarrow I-2)$, using the semiclassical model of Dönau and Frauendorf [21,22], are also included in Fig. 12. The calculations have been performed with both pure single-particle g-factors and also with g-factors taken from cranking calculations [23]; these values are shown in Table IV. The biggest difference occurs for the calculations appropriate for Bands 1/2 which involve a mixed $h_{9/2}/f_{7/2}$ neutron orbital (the $[521]3/2^-$ and $[523]5/2^-$ Nilsson states).

The large theoretical $B(M1)/B(E2)$ values calculated for the $\nu i_{13/2} \otimes \pi\{[523]7/2^- \otimes [404]7/2^+\}_{K=7}$ configuration reproduce the values for Bands 9/10 quite well. Furthermore, the calculations predict positive $E2/M1$ multipole mixing ratios for this configuration, which is consistent with the small A_2 values (see Table I) extracted for the $\Delta I = 1$ transitions

TABLE IV. Orbitals and g factors used to calculate $B(M1)/B(E2)$ ratios of reduced transition probabilities.

Shell-model state	g factor[a]	Nilsson orbital	g factor[b]
$\nu i_{13/2}$	−0.18	$[651]3/2^+$	−0.32
$\nu f_{7/2}$	−0.33	$[521]3/2^-$	−0.20
$\nu h_{9/2}$	0.21	$[523]5/2^-$	0.09
$\pi h_{11/2}$	1.21	$[523]7/2^-$	1.34
$\pi g_{7/2}$	0.74	$[404]7/2^+$	0.62

[a]Pure single-particle g factor calculated with a 60% spin quenching factor.
[b]Taken from cranking calculations.

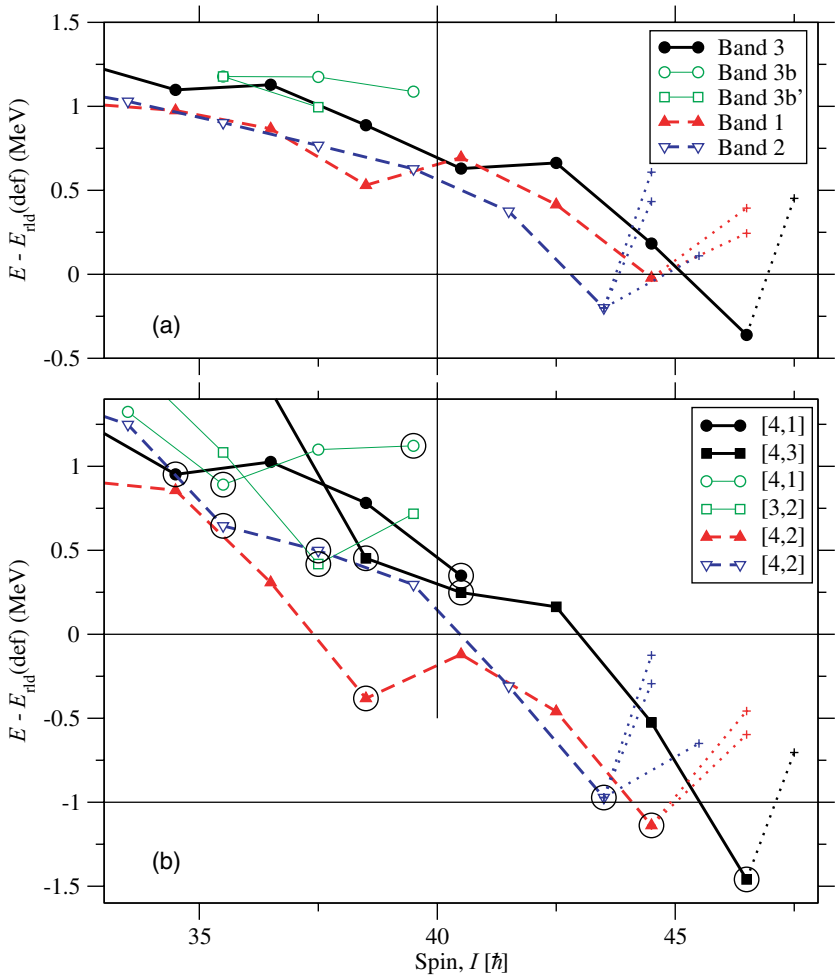

FIG. 13. (Color online) Experimental (a) and theoretical (b) energy relative to a rotating liquid-drop reference for the terminating bands in ^{157}Er, with the non-collective aligned states encircled in panel (b). The lowest observed and calculated states feeding the terminating states are drawn by crosses and dotted lines.

connecting Bands 9 and 10. Calculated $B(M1)/B(E2)$ values for the $\nu[521]3/2^- \otimes (\nu i_{13/2})^2$ and $\nu[523]5/2^- \otimes (\nu i_{13/2})^2$ configurations are compared with the experimental values obtained for Bands 1 and 2. The former configuration is predicted to have negative $E2/M1$ multipole-mixing ratios, while the latter configuration is predicted to have positive $E2/M1$ multipole-mixing ratios above spin $\sim 20\hbar$. The low A_2 angular-distribution coefficients for the 290, 312, and 339 keV transitions (see Table I) linking Bands 1 and 2 imply positive multipole-mixing ratios and confirm the high-spin structure of Bands 1/2 as $\nu[523]5/2^- \otimes (\nu i_{13/2})^2$ (note Band 6 is associated with the $\nu[521]3/2^-$ orbital [17]).

B. High-spin structure

At very high spin, energetically favored terminating states have been observed in ^{157}Er, see also Refs. [7,11]. Figure 13(a) plots the experimental excitation energies for Bands 1–3 relative to a rotating liquid-drop reference [25]; the energetically favored nature of the three terminating states at $87/2^-$, $89/2^-$, and $93/2^+$ is clearly evident. Two of these states were previously observed in Ref. [7] while the third was predicted. They are formed by coupling the eleven valence particles outside the ^{146}Gd core; the $\pi\{(h_{11/2})^4\}_{16^+}$ proton configuration is coupled to the $\nu\{(i_{13/2})^2(h_{9/2}, f_{7/2})^5\}_{55/2^-,57/2^-}$ and $\nu\{(i_{13/2})^3(h_{9/2}, f_{7/2})^4\}_{61/2^+}$ neutron configurations, respectively.

Theoretical configurations are compared with the experimental bands in Fig. 13. The calculations were performed in the framework of the configuration-dependent cranked Nilsson-Strutinsky formalism without pairing [8,24]. The main ingredients of the configurations are $h_{11/2}$ protons and $i_{13/2}$ neutrons; the configurations are thus labeled as $[p_1, n_1]$ where p_1 represents the number of $\pi h_{11/2}$ particles and n_1 the number of $\nu i_{13/2}$ particles. The experimental Bands 1 and 2 are assigned to [4,2] configurations. Band 3 is assigned to [4,1] in the spin range $34.5-40.5\hbar$ and to [4,3] in the spin range $40.5-46.5\hbar$, i.e., the $40.5\hbar$ state is probably a mixture of these two configurations. The $81/2^+$ and $93/2^+$ states are the maximum spin-parity values for these configurations, respectively. In the $69/2^+$ [4,1] state and in the $81/2^+$ [4,3] state, one neutron spin vector is anti-aligned. The levels labeled Bands 3b and 3b′ in Fig. 3 represent positive-parity states with the signature $\alpha = -1/2$. Theoretically it is difficult to construct high-spin terminating configurations for this parity and signature because with an odd number of $i_{13/2}$ neutrons, signature $\alpha = +1/2$ is strongly favored. However, the [3,2] configuration (with one $d_{3/2}$ proton) has a favored $75/2^+$ state with one neutron anti-aligned that could correspond to the

$(75/2^+)$ state of Band 3b′. Similarly a [4,1] configuration could be attributed to Band 3b. This configuration, with signature $\alpha = 1$ for the six $(h_{9/2}, f_{7/2})$ neutrons, has a maximum spin-parity of $79/2^+$ and a favored state at $75/2^+$ when one neutron is antialigned.

The calculations have also been used to understand the nature of the high lying states feeding the terminating states in ^{157}Er. The favored way found to make higher-spin states for $I = 45-55\hbar$ is to excite protons from the $g_{7/2}$ and $d_{5/2}$ orbitals below the $Z = 64$ shell gap into the 5$^{\text{th}}$ and 6$^{\text{th}}$ $h_{11/2}$ orbitals and into the two lowest $d_{3/2}$ orbitals. A systematic investigation has been carried out for these 'core-excited' proton configurations with 1–4 particles excited across the $Z = 64$ gap, as discussed in Ref [11]. There is good qualitative agreement between theory and experiment for these states lying above the terminating states in ^{157}Er. Thus, the energy of the lowest states drawn in in Fig. 13 at the highest spins are similar in experiment and calculations. Furthermore, the calculations give a rather high level density above these lowest states which appears consistent with experiment although it has been possible to fix spin and parity vlues for only a few feeding states. Furthermore, only around 50% of the total feeding intensity is experimentally accounted for. The calculations also suggest that strongly deformed bands should exist at very high spin and evidence has indeed been found for such structures [26].

IV. CONCLUSIONS

A high-statistics, high-spin experiment has been performed in order to study the level structure of ^{157}Er. Many new transitions have been established along with definitive spin-parity level assignments from an angular-distribution analysis. A third energetically favored band-terminating state has been established in this nucleus at $I^\pi = 93/2^+$ in addition to the previously known terminating states at $I^\pi = 87/2^-$ and $89/2^-$. A large number of weak transitions of energies 1.0–2.5 MeV has been identified feeding these terminating states. The details of the high-spin states up to the terminating states are well understood from comparisons with cranked Nilsson-Strutinsky calculations. These calculations indicate that the feeding transitions originate from weakly deformed configurations involving core-breaking proton particle-hole excitations across the semi-magic $Z = 64$ shell gap.

ACKNOWLEDGMENTS

We are indebted to Dr. D. C. Radford for providing the RADWARE analysis codes. This work was supported in part by the United Kingdom Engineering and Physical Sciences Research Council, the U.S. Department of Energy under Contract No. AC03-76SF00098, the National Science Foundation, the State of Florida, and the Swedish Science Research Council.

[1] A. Bohr and B. R. Mottelson, *Nuclear Structure Vol. II* (W. A. Benjamin Inc., New York, 1975), and references therein.
[2] I. Ragnarsson, Z. Xing, T. Bengtsson, and M. A. Riley, Phys. Scr. **34**, 651 (1986).
[3] J. Dudek and W. Nazarewicz, Phys. Rev. C **31**, 298 (1985).
[4] T. Bengtsson and I. Ragnarsson, Phys. Scr. **T5**, 165 (1983).
[5] F. S. Stephens, M. A. Deleplanque, R. M. Diamond, A. O. Macchiavelli, and J. E. Draper, Phys. Rev. Lett. **54**, 2584 (1985).
[6] J. Simpson *et al*., Phys. Lett. **B327**, 187 (1994).
[7] S. J. Gale *et al*., J. Phys. G **21**, 193 (1995).
[8] A. V. Afanasjev, D. B. Fossan, G. J. Lane, and I. Ragnarsson, Phys. Rep. **322**, 1 (1999).
[9] K. Heyde, *Basic Ideas and Concepts in Nuclear Physics* (IOP Publishing, Bristol, 1999), p. 53.
[10] S. G. Nilsson and I. Ragnarsson, *Shapes and Shells in Nuclear Structure* (Cambridge University Press, Cambridge, 1995), p. 230.
[11] A. O. Evans *et al*., Phys. Rev. Lett. **92**, 252502 (2004).
[12] I. Y. Lee, Nucl. Phys. **A520**, 641c (1990).
[13] D. C. Radford, Nucl. Instrum. Methods Phys. Res. A **361**, 297 (1995).
[14] D. C. Radford, M. Cromaz, and C. J. Beyer, in *Proceedings of the Nuclear Structure'98 Conference, Gatlinburg, 1998*, edited by C. Baktash AIP Conf. Proc. No. 48 (American Institute of Physics, New York, 1999), p. 570.
[15] C. W. Beausang *et al*., Nucl. Instrum. Methods Phys. Res. A **364**, 560 (1995).
[16] J. Simpson *et al*., J. Phys. G **15**, 643 (1989).
[17] T. B. Brown *et al*., Phys. Rev. C **66**, 064320 (2002).
[18] R. Vlastou *et al*., Nucl. Phys. **A580**, 133 (1994).
[19] J. Simpson, P. A. Butler, P. D. Forsyth, J. F. Sharpey-Schafer, J. D. Garrett, G. B. Hagemann, B. Herskind, and L. P. Ekstrom, J. Phys. G **10**, 383 (1984).
[20] J. Simpson *et al*., Eur. Phys. J. A **1**, 267 (1998).
[21] F. Dönau and S. Frauendorf, in *Proceedings of the Conference on High Angular Momentum Properties of Nuclei, Oak Ridge, 1982*, edited by N. R. Johnson (Harwood Academic, New York, 1983), p. 143.
[22] F. Dönau, Nucl. Phys. **A471**, 469 (1987).
[23] S. Cwiok, J. Dudek, W. Nazarewicz, W. Skalski, and T. Werner, Comput. Phys. Commun. **46**, 379 (1987).
[24] T. Bengtsson and I. Ragnarsson, Nucl. Phys. **A436**, 14 (1985).
[25] B. G. Carlsson and I. Ragnarsson, submitted to Phys. Lett. B (2006).
[26] E. S. Paul *et al*., to be published.